Joseph Egitto[1]
Department of Mechanical Engineering,
Energy Engineering Graduate Program,
University of Massachusetts Lowell,
Lowell, MA 01854
e-mail: Joseph_Egitto@student.uml.edu

Tugba Ceren Gokoglan[1]
Department of Mechanical Engineering,
Energy Engineering Graduate Program,
University of Massachusetts Lowell,
Lowell, MA 01854
e-mail: TugbaCeren_Gokoglan@student.uml.edu

Shyam K. Pahari
Department of Chemistry and Biochemistry,
University of Massachusetts Dartmouth,
North Dartmouth, MA 02747
e-mail: spahari@umassd.edu

Jennifer N. Bolibok
Department of Chemistry and Biochemistry,
University of Massachusetts Dartmouth,
North Dartmouth, MA 02747
e-mail: jbolibok@umassd.edu

Sundar Rajan Aravamuthan
Department of Mechanical Engineering,
Energy Engineering Graduate Program,
University of Massachusetts Lowell,
Lowell, MA 01854
e-mail: SundarRajan_Aravamuthan@uml.edu

Fuqiang Liu
Department of Mechanical Engineering,
Energy Engineering Graduate Program,
University of Massachusetts Lowell,
Lowell, MA 01854
e-mail: fuqiang_liu@uml.edu

Xinfang Jin
Department of Mechanical Engineering,
Energy Engineering Graduate Program,
University of Massachusetts Lowell,
Lowell, MA 01854
e-mail: Xinfang_Jin@uml.edu

Patrick J. Cappillino
Department of Chemistry and Biochemistry,
University of Massachusetts Dartmouth,
North Dartmouth, MA 02747
e-mail: pcappillino@umassd.edu

Ertan Agar[2]
Department of Mechanical Engineering,
Energy Engineering Graduate Program,
University of Massachusetts Lowell,
Lowell, MA 01854
e-mail: Ertan_Agar@uml.edu

Toward High Energy Density Redox Targeting Flow Batteries With a Mushroom-Derived Electrolyte

Among several types of redox flow batteries (RFBs) under development, non-aqueous redox flow batteries (NRFBs) have the potential to approach the energy density of lithium-ion batteries, while maintaining the advantages of flow systems, including ability to decouple power and energy ratings, and thermal stability. Despite their promise, NRFBs suffer from low energy densities because the solubility limitation of redox species in non-aqueous solvents remains relatively lower compared to water. One promising concept for drastically improving the energy density of NRFBs is the utilization of solid charge storage materials, which are reversibly oxidized or reduced in the electrolyte tanks upon interaction with the redox active species (mediators) dissolved in electrolyte (i.e., redox-targeting flow battery (RTFB)). Herein, we demonstrate a RTFB using a highly stable, bio-inspired mediator, vanadium(IV/V)bis-hydroxyiminodiacetate (VBH), coupled with cobalt hexacyanoferrate (CoHCF) as the solid charge storage material. Based on the charge/discharge cycling experiments, the energy capacity was found to be enhanced by ~5x when CoHCF pellets were added into the tank compared to the case without CoHCF. With the pellet approach, up to ~70% of the theoretical capacity of CoHCF were utilized at 10 mA cm^{-2} current density. Sufficient evidence has indicated that this concept utilizing redox-targeting reactions makes it possible to surpass the solubility limitations of the active material, allowing for unprecedented improvements to the energy density of RFBs. [DOI: 10.1115/1.4054697]

Keywords: Amavadin, bio-inspired electrolyte, electrochemical engineering, non-aqueous redox flow battery, redox-targeting reaction, solubility

1 Introduction

Redox flow batteries (RFBs) are considered a prime candidate for addressing the intermittency problem in renewable energy sources, due to their unique architecture that allows for unparalleled scalability and flexibility required for grid integration [1–3]. Unlike

[1]Equal Contribution.
[2]Corresponding author.
Manuscript received March 1, 2022; final manuscript received May 9, 2022; published online July 1, 2022. Assoc. Editor: George Nelson.

traditional batteries, electrolytes of RFBs are stored in external tanks and circulated through an electrochemical reactor [1,4]. The key advantage of these systems is that power generation and energy storage are decoupled. While the volume of electrolyte and the energy rating can be changed to obtain the required capacity, the size of the cell dictates power rating, providing flexibility and modularity [5–7].

Despite their advantages compared to conventional rechargeable batteries, the low energy density of RFBs remains a critical problem, requiring large electrolyte tanks to achieve rather modest energy storage capacities (<50–100 W h L^{-1}) [8–10], which are significantly lower than the typical energy density values of Li-ion batteries [10,11]. This is because the energy density is dependent on the concentration of active species dissolved in electrolytes. Significant effort has been placed toward enhancing the solubility of various active species in electrolyte solutions. Previous work has focused on improving solubility by changing the composition of the supporting electrolyte [12–14], introducing various additives [15–18] and covalent and ionic modification to active species [19]. Other efforts have attempted to expand the stable operating voltage window as a means to enhance the energy density of RFBs. Generally, this requires transitioning to non-aqueous electrolytes [20–28]. The demand for higher energy density systems, pushing towards higher active material concentration, has resulted in higher viscosity in non-aqueous redox flow battery (NRFB) electrolytes which hinders practical applications due to pumping losses and decreased conductivity [29]. Recent estimates suggest electrolyte viscosity no greater than 10–20 cP and conductivity more than 5–10 mS cm^{-1} are necessary for practical implementation [29]. Furthermore, since viscosity generally increases with solution concentration, the optimal condition for the active species, supporting salt, and solvents concentrations may lie below the theoretical maximum, as increases in capacity are offset by performance losses [30].

In order to increase the energy density of RFBs, several innovative approaches have also been proposed. In one approach, introduced by Qing Wang's Group, solid materials, which are indirectly reduced and oxidized in external tanks via soluble redox active species (mediator), are utilized as the primary charge storage media [31–34]. Similar to a typical flow battery operation, the mediator, which is oxidized in one of the electrochemical half-cells, is pumped to the external tanks. Upon interaction with solid charge storage materials in the tank, the mediator is reduced thus transferring charge to the solid charge storage materials [35–39]. As depicted in Fig. 1, during the charge process, the redox mediator at the positive side (denoted as M_1) is oxidized to M_1^+. The oxidized mediator, M_1^+, is then transported to the external tank, where an appropriate solid charge storage material (denoted as S_1) is contained. Upon interacting with the solid charge storage material, M_1^+ is reduced back to M_1, while S_1 is simultaneously oxidized to S_1^+. In the absence of an externally applied overpotential, these redox-targeting reactions occur spontaneously due to a chemical potential difference between the redox mediator and the solid charge storage material. After transferring its charge, the mediator is returned to the electrochemical cell for a new round of reaction. Wang's group has demonstrated this concept (i.e., redox-targeting flow battery (RTFB), see Fig. 1) exclusively using Li-intercalation materials for non-aqueous redox flow lithium batteries, e.g., $FePO_4$ [31–34,36,40,41] and TiO_2 [42] as solid charge storage materials paired with $FcBr_2$/Fc and $CoCp_2/CoCp_2^*$ redox mediators. The same concept has been applied in lithium–sulfur [43] and lithium–oxygen [44,45] flow batteries to address their chronic problems and harness the intrinsic advantages of these flow battery chemistries. The utilization of redox-targeting reactions has also been implemented in aqueous flow batteries [35,46–49]. The viability of polyaniline as a solid charge storage material was investigated using V^{4+}/V^{3+} and Fe^{3+}/Fe^{2+} redox mediators at negative and positive half-cells, respectively [46]. The same group also demonstrated the utilization of copper hexacyanoferrate as a solid capacity booster in the positive side of a Zn/TEMPTMA RFB [47]. Very recently, a new strategy was introduced based on building a redox active organic molecule into an insoluble polymer to develop mediator/solid storage material pairs with inherently matched standard potentials [50]. Overall, the RTFB has the potential to reach significantly higher energy density than conventional RFBs. This approach can also eliminate the practical issues associated with the high viscosity of concentrated NRFB electrolytes, such as electrolyte flowability and high pumping power losses.

Identification of a suitable redox mediator is a critical initial step for the rational design of RTFBs. Our team has introduced a bio-inspired redox active material based on a molecule known as Amavadin that naturally occurs in mushrooms of the Amanita genus [51,52]. Natural selection pressures on these organisms have shut down decomposition mechanisms by chelating vanadium ions extraordinarily tightly and with high specificity. This compound exhibits the highest stability constant ever measured for a vanadium(iv) ion, with a log equilibrium constant (log K_{eq}) of 23 [53]. Synthetic analogs of Amavadin are synthesized in our labs (vanadium(iv) bis-hydroxyiminodiacetate ($[VBH]^{2-}$)), using inexpensive reagents, at large scale, with high yield [11].

Previous studies demonstrate excellent active material stability of [VBH] both in a static cell and flow battery architecture with increased solubility [11,28,51,52]. Prior work investigating [Ca][VBH] as a NRFB active material was restricted to low

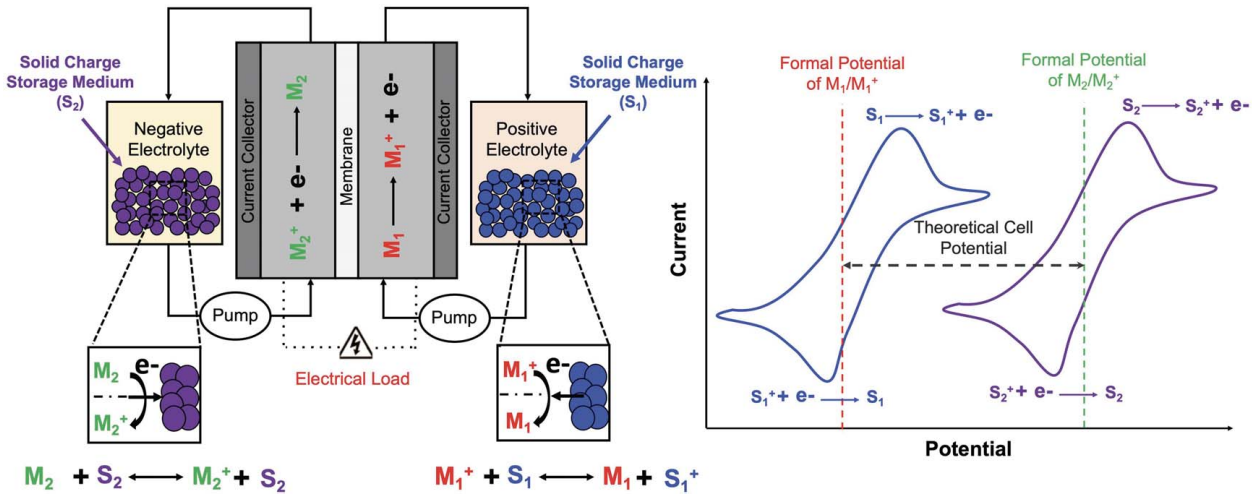

Fig. 1 Schematic of a redox-targeting flow battery with the reactions occurring during operation

concentration in dimethylsulfoxide because this active material exhibits almost no solubility in other non-aqueous solvents [51]. Replacing Ca^{2+} with alkylammonium cations ($[N_{XXXX}]_2$[VBH] compounds (x = 1–4)) exhibited greatly improved solubility (e.g., ~1 M in acetonitrile (MeCN)) [28,52]. O*perando* ultraviolet–visible (UV–vis) spectroscopy was used to provide evidence of tight coupling between redox events and change in concentration of [VBH] during deep flow-cell cycling, illustrating excellent redox stability during cycling operation [11].

Herein, we demonstrate a RTFB using the bio-inspired electrolyte and a suitable solid storage material to provide evidence that the addition of a compatible solid material greatly improves the energy density. To accomplish this objective, a highly stable [VBH] is selected as the redox active material. Owing to its inherent stability (i.e., no interference from side reactions), [VBH] as a testbed allows the detailed analysis required for the elucidation of the redox-targeting reactions between the solid storage and redox active materials. For the solid storage material, cobalt hexacyanoferrate (CoHCF), a Prussian blue analog, was selected based on its formal potential reported in the literature [54]. The formal potential of CoHCF in aprotic electrolytes for sodium ion batteries was reported as ~0.33–0.41 V versus SHE [54], which is in a similar formal potential range (~0.3 V versus SHE [51]) of $[VBH]^{2-}/[VBH]^{1-}$ ($V^{4+}BH/V^{5+}BH$). After sufficient evidence of improvement in the capacity was established, the solid charge storage concept was optimized at system level to further improve the energy density. The performance characteristics of the RFBs with and without the presence of solid charge storage materials are reported and compared using charge/discharge cycling and utilization analyses.

2 Experimental

2.1 Synthesis of Tetrabutylammonium Vanadium(iv) Bis-Hydroxyiminodiacetate. The VBH-based mediator ($[TBA]_2$[VBH]) was synthesized using the procedure reported in our recent study [52]. The prepared solution was centrifuged at 1750 rpm for 25 min and filtered. Concentration was confirmed using UV–vis spectroscopy.

2.2 Synthesis of Solid Charge Storage Material. CoHCF nanoparticles were synthesized in-house according to the procedure outlined by Zhao et al. [55]. The two reagents required for the synthesis (cobalt (II) nitrate [$Co(NO_3)_2$] and potassium hexacyanoferrate [$K_3Fe(CN)_6$]) were acquired from Strem Chemicals and Beantown Chemical, respectively. An aqueous solution of $Co(NO_3)_2$ was added dropwise to an aqueous solution of $K_3Fe(CN)_6$ under vigorous stirring for 1 h until a molar ratio of Co:Fe was 3:2. During the stirring process, the mixture underwent an apparent color change to a dark brown and purple colloids were formed. The product was then centrifuged, washed with copious amounts of distilled water, dried in a Schlenk line for 36 h and analyzed by infrared (IR) spectroscopy.

CoHCF powder was compressed directly into pellets using a hydraulic press. During initial tests, the pellets were immediately breaking apart when submerged in MeCN. To maintain the mechanical integrity of the pellets required for cycling, CoHCF powder was mixed with polyvinylidene fluoride (PVDF) in *n*-methyl-2-pyrrolidone (NMP) solvent. Pellets were prepared using 80 wt% CoHCF and 20 wt% PVDF binder dissolved in NMP solvent. For each 100 mg CoHCF, 0.5 mL NMP was added into the solid/binder mixture. The solution was stirred in an aluminum plate and sonicated for 8 min. Then, the plate was placed in a vacuum oven at a temperature of 100 °C. The plate was left to dry in the oven overnight. A hydraulic die set was used to compress the dried material into pellets, where the structural stability was tested by placing the pellet in MeCN overnight. The weights of the pellets were measured before each use.

2.3 Flow-Cell Experiment. The flow battery setup employed a flow-cell with two external tanks containing the [VBH] electrolyte solution in each half-cell (symmetric flow-cell). The flow-cell was assembled using two layers of 650 μm carbon cloth electrode (AvCarb—as received), one layer of 1/32 in.-thick silicone gaskets (McMaster Carr), and graphite bipolar plates with interdigitated flow fields on each side of the flow-cell. The electrodes (5 cm^2 geometric area) were compressed to ~58% of their initial thickness when the flow-cell was fully assembled. Nafion XL was chosen as the membrane material and was soaked in MeCN for 24 h before assembly of the flow-cell.

2.4 Ultraviolet–Visible Spectroscopy. The concentration and the state of charge (SOC) of both the positive and negative electrolytes were closely monitored using UV–vis spectroscopy (ThermoFisher Evolution 220) based on the extinction coefficients reported in the literature, 25.2 M^{-1} cm^{-1} ($\lambda = 825$ nm) and 240.1 M^{-1} cm^{-1} ($\lambda = 485$ nm) for $[VBH]^{2-}$ and $[VBH]^{1-}$, respectively [11,52]. Using the measured absorbance of the solution, the concentration of the solution can be determined through the Beer's law. Characterization of each of the half-cells was imperative to this study in order to monitor the stability of the active material (VBH) and to ensure that crossover of mediators through the separator does not contribute to the capacity improvement.

2.5 Cyclic Voltammetry. Cyclic voltammograms (CVs) were recorded in a three-electrode electrochemical cell with a CoHCF coated graphite sheet as the working electrode, plain graphite sheet as the counter electrode and $Ag/AgNO_3$ (10 mM silver nitrate ($AgNO_3$) and 100 mM tetrabutylammonium hexafluorophosphate ($TBAPF_6$) in MeCN) as the non-aqueous reference electrode. A total of 50 mM $TBAPF_6$ was used as the electrolyte. The measurement was obtained between 1.2 V and −0.6 V at 5 mV/s scan rate. For the redox behavior of the mediator, similar CV measurements were conducted in a two-compartment H-cell with 50 mM $[TBA]_2$[VBH] solution in one side and 50 mM $TBAPF_6$ on the other side of the compartment. Plain graphite rods were used as the working and counter electrodes. The potential at which the redox mediator ($[VBH]^{2-}/[VBH]^{1-}$) undergoes redox reactions were determined and compared with the formal potential of the CoHCF determined from the CV measurement.

2.6 Cation Intercalation Experiment. A total of 16.9 mM $[TBA]_2$[VBH] solution was prepared in MeCN. Four vials were loaded with 3 mL of $[TBA]_2$[VBH] and 1 equivalent CoHCF. Variable amount of KPF_6 were added (0, 0.12, 0.5, and 1.0 molar equivalent) to vials 1–4. They were allowed to stir for 1 h and centrifuged at 7000 rpm for 10 min. UV–vis spectra were collected.

3 Results and Discussion

3.1 Energy Capacity Enhancement Using the "Teabag Approach". To validate the capacity booster behavior of the redox-targeting approach, a symmetric flow-cell cycling experiment was designed. The benefits of using a symmetrical flow-cell are that it allows for the simultaneous charging and discharging of the redox active material, as there is only one redox couple present. Another important feature is that any potential crossover of the active material does not result in cross-contamination and thus avoids side reactions that may occur in the flow system [11,56]. To ensure that any measured improvements in the energy density of the flow battery were solely due to the addition of the solid storage material, the positive side of the flow-cell setup was designed as the *capacity limiting side* and the solid charge storage material was only added into the positive tank (see Fig. 2(*a*)). For the cycling experiments, electrolytes with 50% SOC were placed in each tank. The electrolyte in the positive side was initially discharged by ~25% at a constant

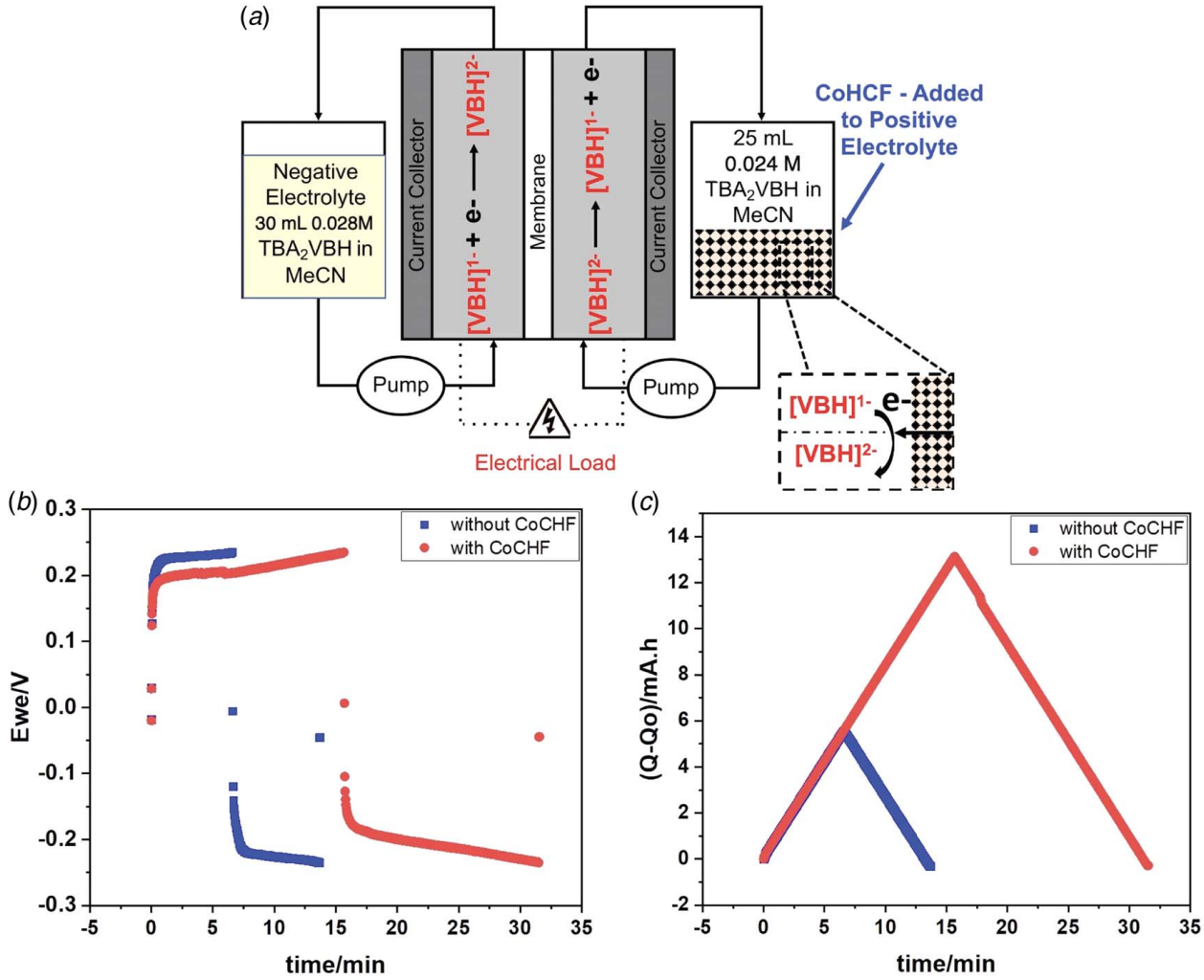

Fig. 2 (*a*) Schematic of the symmetric flow-cell cycling setup—CoHCF powder were added to the (+) tank (capacity limited side), (*b*) cell potential, and (c) the capacity reached during constant current operation (with cutoff voltage) for the setups with/without CoHCF as the charge storage material

current density of 10 mA cm^{-2}. After this initial discharge process, the volumes were measured, and concentrations were determined using UV–vis. After verifying that the concentrations of each half-cell were within the specified ranges, ~50% SOC-depth charge/discharge cycles were performed at a current density of 10 mA cm^{-2}. Charge/discharge durations were initially determined by calculating the 50% capacity of the electrolytes. In order to directly compare the accessed capacity between the cases with and without the solid charge storage material, the cutoff voltage was adjusted between ±0.1–0.5 V after the first cycle so that the assigned cutoff voltage was achieved before the charge/discharge time was reached for both cases with and without the solid charge storage material. After the appropriate cutoff voltage was determined, the cycling process was continued until the charging capacity was stabilized. These steady-state data were used as the baseline for determining the improvement in energy density when solid storage material was added to the flow setup. When steady state was reached, the experiment was stopped, and volume and concentration measurements were taken. Subsequently, CoHCF was placed into the positive tank. The charge/discharge cycling was then continued using the same parameters described above—until steady state was once again reached—typically 8–10 cycles. After completion, the volume and concentration of the electrolytes were measured with UV–vis spectroscopy to detect any fluctuations in active material concentration.

The accessed capacity of the electrolyte (25 mL on the (+) side, 0.024 M [VBH] and 30 mL on (−) side, 0.028 M [VBH] in MeCN) was measured as 6.02 mA h at the current density of 10 mA cm^{-2} with 0.235 V cutoff voltage. This corresponds to 37.4% of the 16.08 mA h theoretical capacity of the electrolyte in the absence of CoHCF. Subsequently, 0.5 g of CoHCF were added to the positive electrolyte tank (*capacity limited side*) using a porous filter apparatus. A funnel was created using the filter and the CoHCF powder was placed into the funnel like a "teabag." Upon cycling of the cell, the accessed capacity was found to be 13.09 mA h with an increase of ~120% compared to the base case (see Figs. 2(*b*) and 2(*c*)), corresponding to *81.4% of the theoretical capacity of the electrolyte alone*. To confirm that the observed increase in capacity is not caused by crossover, the concentration of the positive electrolyte before and after the cycling tests was measured. Shown in Table 1 are the concentrations of active material present in both the positive and negative sides before and after charge/discharge cycling, with and without CoHCF added. Adjusting the maximum theoretical charge capacity by accounting for the losses in active material (0.60–0.46 mmol), the capacity of the electrolyte just before the addition of CoHCF can be calculated as 12.22 mA h. Based on the measured capacity after adding the solid material, the CoHCF utilization was determined to be ~32%. This relatively lower utilization can be attributed to interaction limitations at the solid–liquid interface. Since the solid storage

Table 1 Volume, concentration, % SOC, and number of moles for the positive and negative electrolytes with and without the addition of CoHCF powder

	Without CoHCF		With CoHCF	
	Positive electrolyte	Negative electrolyte	Positive electrolyte	Negative electrolyte
Volume (mL)	25	30	21.5	26
Conc. (mM)	24	28	21.2	36
% SOC	27%	65%	26%	64%
Moles (mmol)	0.60	0.84	0.46	0.94

medium used for this experiment was placed in a filter, the most likely scenario is that not all of the CoHCF interacted with the VBH electrolyte. This limited interaction would still result in an increase in energy density for the system, but the measured value would be less than 50% of the theoretical maximum calculated.

3.2 Energy Capacity Enhancement Using the "Pellet Approach". As seen in Table 1, the volume of electrolyte at the positive side decreased slightly over cycling periods due to the relatively high volatility of acetonitrile and the electrolyte tanks not being fully enclosed when CoHCF was added. Additionally, since this setup employed a filter apparatus to prevent the solid material from circulating through the flow battery system, it was found to be difficult to optimize the electrolyte flowrate for achieving maximum interaction between the electrolyte and the solid charge storage material. Consequently, an additional set of experiments were performed, in which the solid charge storage material was added directly to the positive tank, allowing for maximum interaction between the mediator and charge storage materials and resulting in a higher CoHCF utilization. This was made possible by compressing the CoHCF into disc-shaped pellets that could be directly added to the positive tank.

To provide further evidence that the addition of the solid storage material can surpass the solubility limitations that previously hindered redox flow batteries, similar charge/discharge cycling experiments were conducted using low concentration solutions. The starting solution contained 15 mL of 7 mM VBH electrolyte at the positive side and 9.5 mL of 83 mM electrolyte at the negative side. Since the moles of active material at the negative side were significantly greater than the positive side (7.5 ×-larger), crossover of active material would have a noticeable impact on the capacity of the system. For this reason, the theoretical capacity of the positive side in the absence of CoHCF was taken as the final value, after cycling, and should thus be considered a maximum throughout the experiment. Based on the starting volume and concentration of the positive electrolyte, the initial theoretical capacity of the system (100% SOC-depth) was 2.81 mA h. However, considering the increased concentration measured after charge/discharge cycling without any pellets added (see Table 2), the final theoretical capacity was 4.88 mA h. After addition of a 140 mg (80 wt% CoHCF) pellet, the observed capacity of the flow battery was 6.68 mA h (see Fig. 3), an approximately 370% increase in capacity from the measured value without the pellet and *137% of the theoretical capacity of the positive electrolyte* (see Table 3). The utilization of this pellet was calculated to be ∼80%.

Subsequently, a 129 mg (95 wt% CoHCF) pellet was added to the positive side electrolyte, followed by charge/discharge cycling (using the same assigned cutoff voltage) until steady state was achieved. With the addition of the second pellet (∼122.5 mg CoHCF) to the positive side, the theoretical capacity of the flow battery system was increased by 5.47 mA h. As seen in Fig. 3(*c*), the capacity of the flow system after charge/discharge cycling with both pellets was observed as 8.71 mA h (518% improvement in capacity). Using the calculated theoretical maximum capacity and the observed capacity with the added pellet, the CoHCF utilization for the two pellets together was determined to be ∼70%. The capacity improvement after the addition of the second pellet was determined to be ∼30% based on the measured capacities in Table 3. The observed capacity with the 140 mg pellet, estimated on a volumetric- and molar-base, was then used to determine the capacity improvement from adding the second pellet. Adjusting the measured volumetric- and molar-base capacities based on the volume and moles of active material measured after charge/discharge cycling with both pellets, the improvement was calculated to be 64% and 5.6%, respectively (see Table 3). The lower capacity improvement on the mole base is due to the increase in moles of active material, either due to crossover or from absorbed electrolyte in the pellet from previous experiments. After charge/discharge cycling with the two pellets added to the positive side was completed, volume and concentration measurements were taken, where it was once again observed that the moles of active material in the positive side increased over the cycling period. The increase in the moles of active material could either be from crossover due to the large gradient between the positive and negative sides or from some of the active material staying absorbed in the pellet from previous charge/discharge cycling experiment.

3.3 Matching Standard Potentials Between the Mediator and the Solid Charge Storage Material. The operation of RTFBs requires two key processes in sequence: (i) the mediators should be transported to a reaction site in the tank by means of convection and diffusion and (ii) an electron transfer (often coupled with another process such as cation intercalation) has to be initiated. During the second process, the redox mediator provides the chemical overpotential needed to charge/discharge the active material. Thus, the mediator should provide a chemical potential sufficient to drive oxidation or reduction of the charge storage material. In certain cases, as seen in our system, it may be possible to drive both reactions with a single redox mediator, provided the formal potential of the redox mediator and the active material closely match. Surprisingly, despite the fact that literature suggests that $[TBA]_2[VBH]$ and CoHCF have similar reduction potentials (∼0.3 versus SHE) [51,54], investigation of the cyclic voltammetry of the CoHCF and $[TBA]_2[VBH]$ used to carry out the

Table 2 Concentration and volume measurements of the electrolytes before and after charge/discharge cycling without added pellets, with the addition of the ∼140 mg pellet (80 wt% CoHCF, 20 wt% PVDF), and with the additional ∼129 mg pellet (95 wt% CoHCF, 5 wt% PVDF)

	Starting point		After eight cycles (before adding pellets)		After 19 cycles (with 140 mg pellet)		After 16 cycles (with 140 mg + 129 mg pellets)	
	Positive	Negative	Positive	Negative	Positive	Negative	Positive	Negative
Volume (mL)	15	9.5	14	9.5	12.5	10.5	10	10.5
Conc. (mM)	7.0	85	13	83	13.3	55	21	45
% SOC	37%	64%	26%	64%	17%	82%	43%	78%
Moles (mmol)	0.11	0.79	0.18	0.79	0.17	0.58	0.21	0.47

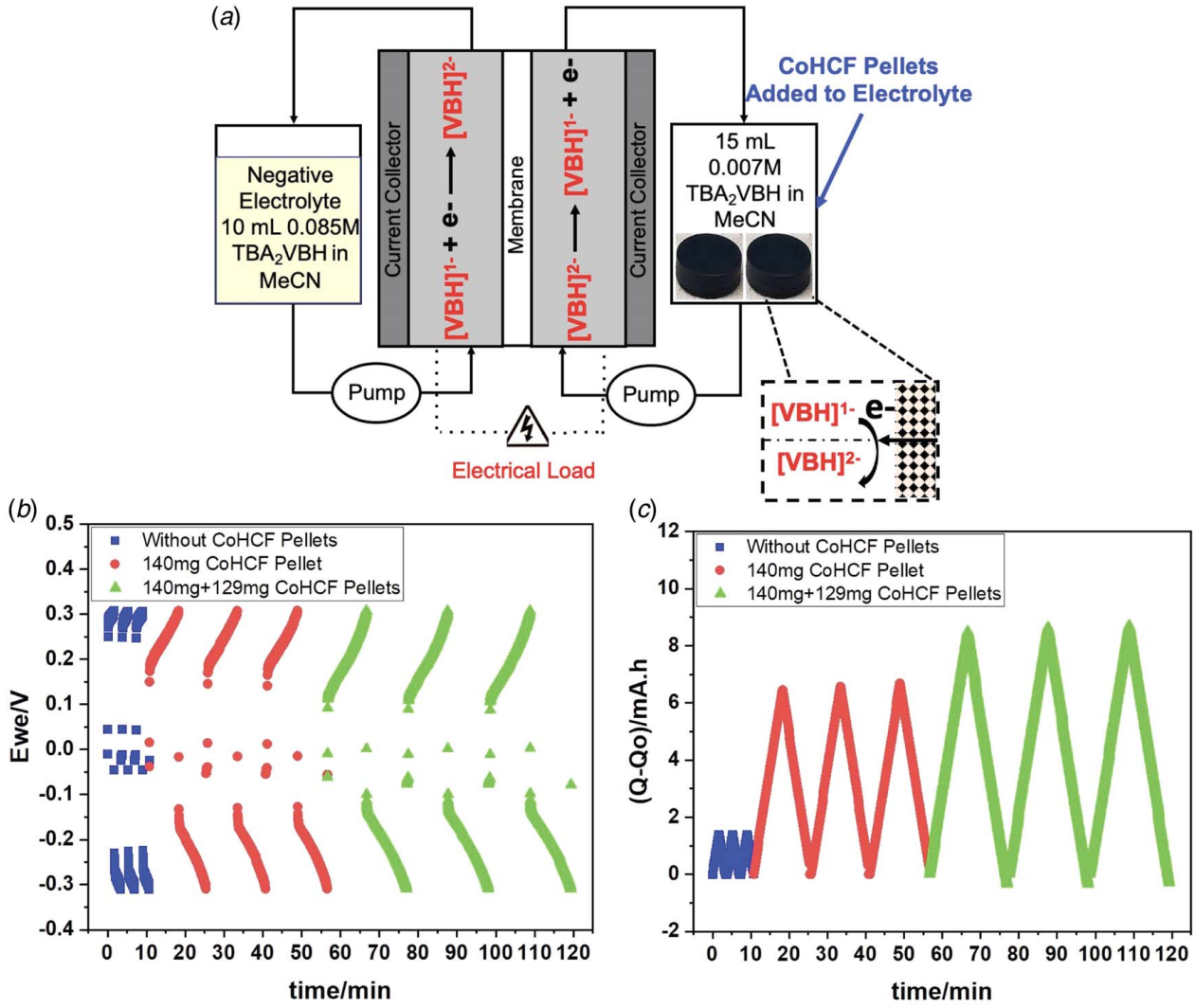

Fig. 3 (*a*) Schematic of a symmetric flow-cell setup—CoHCF pellets were added to the (+) tank (capacity limited side), (*b*) cell potential, and (*c*) the capacity reached during constant current operation (with cutoff voltage) for the setups with/without CoHCF as the charge storage material

targeted-flow experiments showed a discrepancy between the standard potentials (see Fig. 4(*a*)). The apparent contradiction between the observed reversibility of the VBH/CoHCF target-flow system and the difference between observed formal potentials can be rectified by considering the effect of cation intercalation during CoHCF reduction [19]. It is clear from the literature that the standard potential of redox intercalation changes considerably depending on the size of counter cation [57,58]. For example, Sinha et al. report an approximately 480 mV positive shift for NiHCF going from small, Li^+ cations to large, Cs^+ cations [57]. Furthermore, a recent, combined, Raman, in situ, powder X-ray diffraction study showed that reduction of $A[Fe^{3+}Fe^{2+}(CN)_6]$, where $A = Na^+$ or K^+, follows a solid-solution mechanism, where the reduction potential varies smoothly as the lattice expands during cation intercalation, in the case of Na^+, but undergoes a sharp transition to a second crystal phase, in the case of K^+ intercalation [19]. We also note that the stoichiometry of CoHCF is promiscuous and prone to small variations, including the incorporation of small amounts of K^+ carried over during synthesis [59]. We hypothesized that even substoichiometric quantities of adventitious K^+ could

Table 3 Observed and theoretical capacities of the electrolyte with and without the addition of ~140 mg pellet (80 wt% CoHCF, 20 wt% PVDF binder) and added ~129 mg pellet (95 wt% CoHCF, 5 wt% PVDF binder) to the positive tank originally containing 15 mL of 7 mM VBH electrolyte

	Theoretical capacity (mA h)	Measured capacity (mA h)	Measured volumetric capacity (mA h mL^{-1})	Measured molar capacity (mA h $mmol^{-1}$)
Without CoHCF	4.88	1.41	0.10	7.83
With 140 mg pellet	9.45	6.68	0.53	39.29
With 140 mg + 129 mg pellets	16.09	8.71	0.87	41.48
Total capacity added	11.21	7.30	0.77	33.65

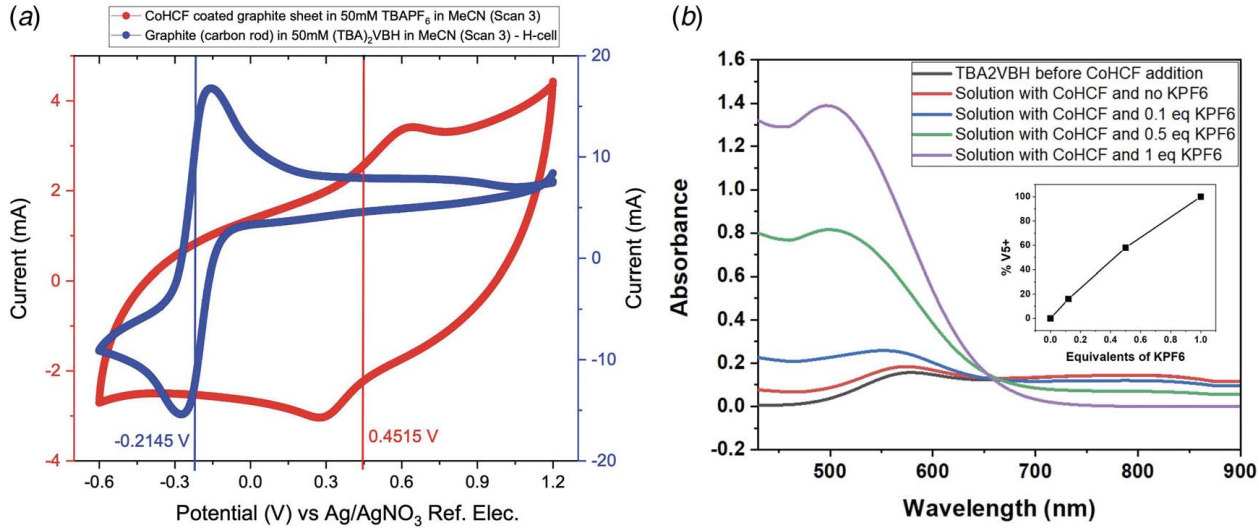

Fig. 4 (*a*) Cyclic voltammograms of CoHCF coated graphite sheet in 50 mM TBAPF6 in MeCN compared with the CVs of graphitic carbon rod in 50 mM $(TBA)_2VBH$ in MeCN and (*b*) UV–vis spectra of $(TBA)_2VBH$ solution before and after the addition of CoHCF and with various concentration of KPF_6 salt

modulate the formal potential of CoHCF, establishing an equilibrium between reduced and oxidized VBH that accounts for the observed reversibility. To investigate this, samples of 17 mM $[TBA]_2[VBH]$ in acetonitrile were stirred for 1 h with one equivalent of CoHCF and quantities of KPF_6 ranging from zero to one equivalent. As shown in Fig. 4(*b*), in the absence of added K^+, a stirred solution of $V^{4+}BH$ is stable, experiencing less than 1% oxidation to $V^{5+}BH$. Additional quantities of KPF_6 gradually shift the $V^{4+/5+}$ equilibrium until quantitative oxidation to $V^{5+}BH$ is observed after addition of one equivalent of KPF_6. To verify the presence of K^+ in the CoHCF powder synthesized, IR spectra of contaminated CoHCF, pure CoHCF, KNO_3, and the subtraction of contaminated CoHCF–pure CoHCF were obtained and shown in Fig. 5. Since the subtracted IR spectrum looks identical to the spectrum of KNO_3, it is evident that KNO_3 is present in the CoHFC powder.

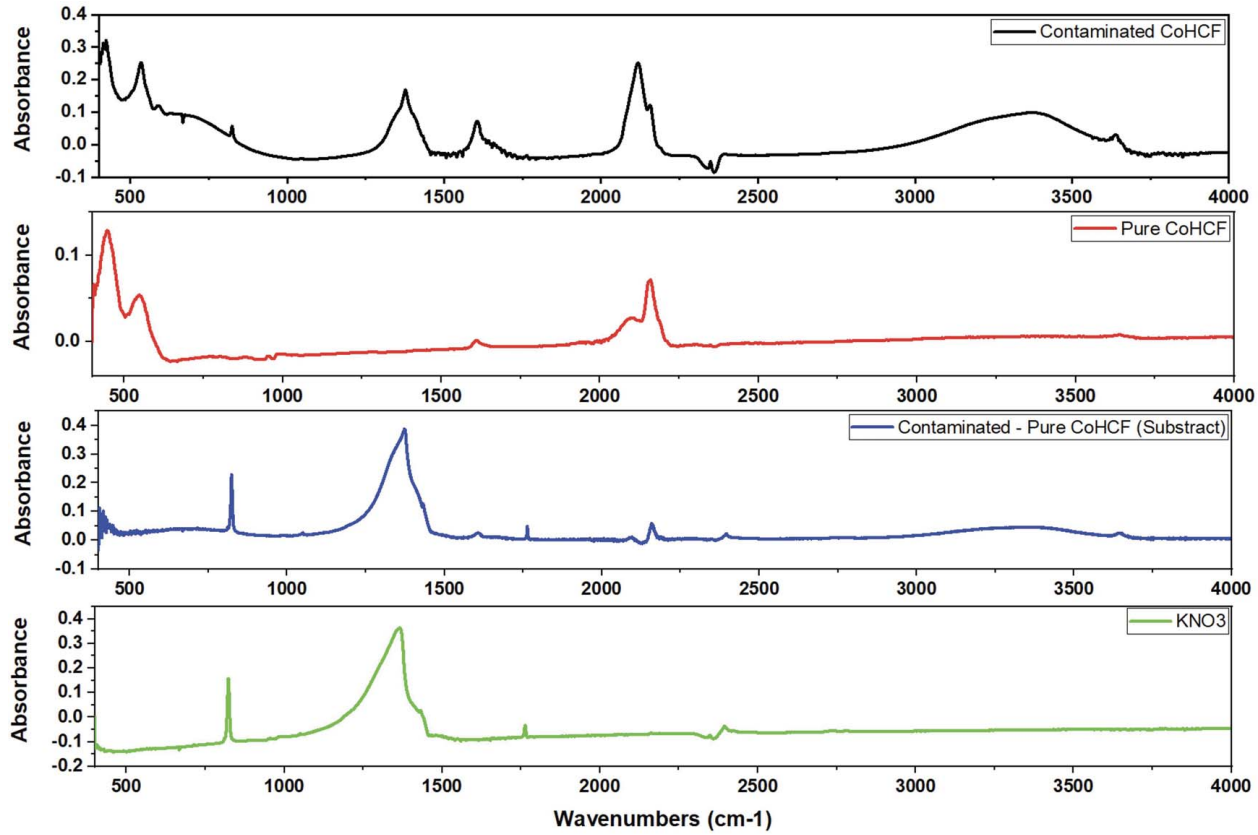

Fig. 5 Infrared spectra of contaminated CoHCF, pure CoHCF, the subtraction of contaminated CoHCF, pure CoHCF, and KNO_3

4 Conclusion

In summary, RTFB based on the high-stability [VBH] active material coupled with CoHCF as the solid charge storage material allowed for the energy density of the flow battery to be greatly improved. To determine the capacity improvements during cycling made by CoHCF on the flow system, a cutoff voltage was assigned based on the potential observed at 50% SOC-depth of the capacity limiting side (positive electrolyte) without CoHCF. This ensured that when CoHCF was added to the positive side, the observed capacity could be directly compared to the measured capacity of the flow battery without CoHCF. Since the cutoff voltage remained constant with and without CoHCF, i.e., the same boundary conditions were applied, any capacity improvement would therefore be a direct result of the addition of the solid material.

The initial design for the redox mediation concept was based on a flow through concept, which is operated by having the oxidized electrolyte at the positive side flowing through the solid charge storage material (teabag approach). Although evidence has shown that this design improved the energy density of the system, many parameters needed to be controlled which increased the complexity of the system. Therefore, an alternative approach was devised which focused on the direct addition of CoHCF to the positive side to reduce complexity while still maintaining a high interaction at the solid–liquid interface. In this method, CoHCF powder was compressed into 10 mm diameter pellets that could be directly added to the positive tank (pellet approach)—a far less complex approach than the previously mentioned flow through concept. These pellets were capable of utilizing up to ~70% of the available capacity from CoHCF and improve the energy density by ~5 ×. As more pellets were added to the positive side, the capacity of the flow battery was found to increase further, meaning that the capacity is limited by the amount of solid charge storage material in the electrolyte tank and their utilization with the electrolyte. Sufficient evidence has indicated that this redox mediation concept makes it possible to surpass the solubility limitations of the active material, allowing for unprecedented improvements to the energy density of RFBs. Furthermore, observations obtained from the cation intercalation experiment, taken together with the reversibility of the VBH/CoHCF system, demonstrate that an empirical approach to matching RTFB mediators with solid charge storage materials may be most effective. Furthermore, they suggest a promising strategy for optimizing RTFB performance, by altering the ratio of a combination of supporting cations with various intercalation potential, which is currently under investigation.

Acknowledgment

The authors gratefully acknowledge Department of Navy Award N00014-20-1-2858 issued by the Office of Naval Research (ONR) for supporting this study. The authors would also like to thank AvCarb Materials Solutions for providing electrode materials. This research was supported in part by UMass Dartmouth's Marine and Undersea Technology (MUST) Research Program funded by the Office of Naval Research (ONR) under Grant No. N00014-20-1-2170.

Conflict of Interest

There are no conflicts of interest.

Data Availability Statement

The datasets generated and supporting the findings of this article are obtainable from the corresponding author upon reasonable request.

References

[1] Soloveichik, G. L., 2015, "Flow Batteries: Current Status and Trends," Chem. Rev., **115**(20), pp. 11533–11558.

[2] Gong, K., Fang, Q., Gu, S., Li, S., and Yan, Y., 2015, "Nonaqueous Redox-Flow Batteries: Organic Solvents, Supporting Electrolytes, and Redox Pairs," Energy Environ. Sci., **8**(12), pp. 3515–3530.

[3] Sánchez-Díez, E., Ventosa, E., Guarnieri, M., Trovò, A., Flox, C., Marcilla, R., Soavi, F., Mazur, P., Aranzabe, E., and Ferret, R., 2021, "Redox Flow Batteries: Status and Perspective Towards Sustainable Stationary Energy Storage," J. Power Sources, **481**, p. 228804.

[4] Weber, A. Z., Mench, M. M., Meyers, J. P., Ross, P. N., Gostick, J. T., and Liu, Q., 2011, "Redox Flow Batteries: A Review," J. Appl. Electrochem., **41**(10), pp. 1137–1164.

[5] García-Salaberri, P. A., Gokoglan, T. C., Ibáñez, S. E., Agar, E., and Vera, M., 2020, "Modeling the Effect of Channel Tapering on the Pressure Drop and Flow Distribution Characteristics of Interdigitated Flow Fields in Redox Flow Batteries," Processes, **8**(7), p. 775.

[6] Nourani, M., Zackin, B. I., Sabarirajan, D. C., Taspinar, R., Artyushkova, K., Liu, F., Zenyuk, I. V., and Agar, E., 2019, "Impact of Corrosion Conditions on Carbon Paper Electrode Morphology and the Performance of a Vanadium Redox Flow Battery," J. Electrochem. Soc., **166**(2), pp. A353–A363.

[7] Nourani, M., Dennison, C. R., Jin, X., Liu, F., and Agar, E., 2019, "Elucidating Faradaic Imbalance on Vanadium Redox Flow Battery Performance: Experimental Characterization," J. Electrochem. Soc., **166**(15), pp. A3844–A3851.

[8] VanGelder, L. E., and Matson, E., 2018, "Heterometal Functionalization Yields Improved Energy Density for Charge Carriers in Nonaqueous Redox Flow Batteries," J. Mater. Chem. A, **6**(28), pp. 13874–13882.

[9] Leung, P., Shah, A. A., Sanz, L., Flox, C., Morante, J. R., Xu, Q., Mohamed, M. R., Ponce de Leoń, C., and Walsh, F. C., 2017, "Recent Developments in Organic Redox Flow Batteries: A Critical Review," J. Power Sources, **360**, pp. 243–283.

[10] Wei, X., Pan, W., Duan, W., Hollas, A., Yang, Z., Li, B., Nie, Z., et al., 2017, "Materials and Systems for Organic Redox Flow Batteries: Status and Challenges," ACS Energy Lett., **2**(9), pp. 2187–2204.

[11] Gokoglan, T. C., Pahari, S. K., Hamel, A., Howland, R., Cappillino, P. J., and Agar, E., 2019, "Operando Spectroelectrochemical Characterization of a Highly Stable Bioinspired Redox Flow Battery Active Material," J. Electrochem. Soc., **166**(10), pp. A1745–A1751.

[12] Vijayakumar, M., Wei, W., Zimin, N., Sprenkle, V., and JianZhi, H., 2013, "Elucidating the Higher Stability of Vanadium (V) Cations in Mixed Acid Based Redox Flow Battery Electrolytes," J. Power Sources, **241**, pp. 173–177.

[13] Wen, Y. H., Xu, Y., Cheng, J., Cao, G. P., and Yang, Y. S., 2013, "Investigation on the Stability of Electrolyte in Vanadium Flow Batteries," Electrochim. Acta, **96**, pp. 268–273.

[14] Wu, X. W., Liu, J., Xiang, X. J., Zhang, J., Hu, J. P., and Wu, Y. P., 2014, "Electrolytes for Vanadium Redox Flow Batteries," Pure Appl. Chem., **86**(5), pp. 661–669.

[15] Zhang, J., Li, L., Nie, Z., Chen, B., Vijayakumar, M., Kim, S., Wang, W., Schwenzer, B., Liu, J., and Yang, Z., 2011, "Effects of Additives on the Stability of Electrolytes for All-Vanadium Redox Flow Batteries," J. Appl. Electrochem., **41**(10), pp. 1215–1221.

[16] Wang, G., Chen, J., Wang, X., Tian, J., Kang, H., Zhu, X., Zhang, Y., Liu, X., and Wang, R., 2013, "Influence of Several Additives on Stability and Electrochemical Behavior of V (V) Electrolyte for Vanadium Redox Flow Battery," J. Electroanal. Chem., **709**, pp. 31–38.

[17] Wang, G., Chen, J., Wang, X., Tian, J., Kang, H., Zhu, X., Zhang, Y., Liu, X., and Wang, R., 2014, "Study on Stabilities and Electrochemical Behavior of V (V) Electrolyte With Acid Additives for Vanadium Redox Flow Battery," J. Energy Chem., **23**(1), pp. 73–81.

[18] Lei, Y., Liu, S.-Q., Gao, C., Liang, X.-X., He, Z.-X., Deng, Y.-H., and He, Z., 2013, "Effect of Amino Acid Additives on the Positive Electrolyte of Vanadium Redox Flow Batteries," J. Electrochem. Soc., **160**(4), pp. A722–A727.

[19] Piernas, M. J., and Martínez, E. C., 2018, "Chapter 2: Prussian Blue and Its Analogues. Structure, Characterization and Applications," *Prussian Blue Based Batteries*, Springer, pp. 9–22.

[20] Attanayake, N. H., Kowalski, J. A., Greco, K. V., Casselman, M. D., Milshtein, J. D., Chapman, S. J., Parkin, S. R., Brushett, F. R., and Odom, S. A., 2019, "Tailoring Two-Electron-Donating Phenothiazines to Enable High Concentration Redox Electrolytes for Use in Nonaqueous Redox Flow Batteries," Chem. Mater., **31**(12), pp. 4353–4363.

[21] Saraidaridis, J. D., and Monroe, C. W., 2019, "Nonaqueous Vanadium Disproportionation Flow Batteries With Porous Separators Cycle Stably and Tolerate High Current Density," J. Power Sources, **412**, pp. 384–390.

[22] Cappillino, P. J., Pratt, H. D., Hudak, N. S., Tomson, N. C., Anderson, T. M., and Anstey, M. R., 2014, "Application of Redox Non-Innocent Ligands to Non-Aqueous Flow Battery Electrolytes," Adv. Energy Mater., **4**(1), p. 1300566.

[23] Sevov, C. S., Hickey, D. P., Cook, M. E., Robinson, S. G., Barnett, S., Minteer, S. D., Sigman, M. S., and Sanford, M. S., 2017, "Physical Organic Approach to Persistent, Cyclable, Low-Potential Electrolytes for Flow Battery Applications," J. Am. Chem. Soc., **139**(8), pp. 2924–2927.

[24] Kucharyson, J. F., Cheng, L., Tung, S. O., Curtiss, L. A., and Thompson, L. T., 2017, "Predicting the Potentials, Solubilities and Stabilities of Metal-Acetylacetonates for Non-Aqueous Redox Flow Batteries Using Density Functional Theory Calculations," J. Mater. Chem. A, **5**(26), pp. 13700–13709.

[25] Zhao, Y., Zhang, J., Agarwal, G., Yu, Z., Corman, R. E., Wang, Y., Robertson, L. A., et al., 2021, "TEMPO Allegro: Liquid Catholyte Redoxmers for Nonaqueous Redox Flow Batteries," J. Mater. Chem. A, **9**(31), pp. 16769–16775.

[26] Attanayake, N. H., Suduwella, T. M., Yan, Y., Kaur, A. P., Liang, Z., Sanford, M. S., and Odom, S. A., 2021, "Comparative Study of Organic Radical Cation Stability and Columbic Efficiency for Nonaqueous Redox Flow Battery Applications," J. Phys. Chem. C, **125**(26), pp. 14170–14179.
[27] Liu, B., Tang, C. W., Zhang, C., Jia, G., and Zhao, T., 2021, "Cost-Effective, High-Energy-Density, Nonaqueous Nitrobenzene Organic Redox Flow Battery," Chem. Mater., **33**(3), pp. 978–986.
[28] Visayas, B. R. B., Pahari, S. K., Gokoglan, T. C., Golen, J. A., Agar, E., Cappillino, P. J., and Mayes, M. L., 2021, "Computational and Experimental Investigation of the Effect of Cation Structure on the Solubility of Anionic Flow Battery Active-Materials," Chem. Sci., **12**(48), pp. 15892–15907.
[29] Shkrob, I. A., Robertson, L. A., Yu, Z., Assary, R. S., Cheng, L., Zhang, L., Sarnello, E., et al., 2021, "Crowded Electrolytes Containing Redoxmers in Different States of Charge: Solution Structure, Properties, and Fundamental Limits on Energy Density," J. Mol. Liq., **334**, p. 116533.
[30] Barton, J. L., Milshtein, J. D., Hinricher, J. J., and Brushett, F. R., 2018, "Quantifying the Impact of Viscosity on Mass-Transfer Coefficients in Redox Flow Batteries," J. Power Sources, **399**, pp. 133–143.
[31] Huang, Q., Li, H., Grätzel, M., and Wang, Q., 2013, "Reversible Chemical Delithiation/Lithiation of $LiFePO_4$: Towards a Redox Flow Lithium-Ion Battery," Phys. Chem. Chem. Phys., **15**(6), pp. 1793–1797.
[32] Huang, Q., Yang, J., Ng, C., Jia, C., and Wang, Q., 2016, "A Redox Flow Lithium Battery Based on the Redox Targeting Reactions Between $LiFePO_4$ and Iodide," Energy Environ. Sci., **9**(3), pp. 917–921.
[33] Jia, C., Pan, F., Zhu, Y., Huang, Q., Lu, L., and Wang, Q., 2015, "High-Energy Density Nonaqueous All Redox Flow Lithium Battery Enabled With a Polymeric Membrane," Sci. Adv., **1**(10), p. e1500886.
[34] Jennings, J. R., Huang, Q., and Wang, Q., 2015, "Kinetics of $LixFePO_4$ Lithiation/Delithiation by Ferrocene-Based Redox Mediators: An Electrochemical Approach," J. Phys. Chem. C, **119**(31), pp. 17522–17528.
[35] Gentil, S., Reynard, D., and Girault, H., 2020, "Aqueous Organic and Redox-Mediated Redox Flow Batteries: A Review," Curr. Opin. Electrochem., **21**, pp. 7–13.
[36] Yan, R., and Wang, Q., 2018, "Redox-Targeting-Based Flow Batteries for Large-Scale Energy Storage," Adv. Mater., **30**(47), p. 1802406.
[37] Moghaddam, M., Sepp, S., Wiberg, C., Bertei, A., Rucci, A., and Peljo, P., 2021, "Thermodynamics, Charge Transfer and Practical Considerations of Solid Boosters in Redox Flow Batteries," Molecules, **26**(8), p. 2111.
[38] Wang, X., Zhou, M., Zhang, F., Zhang, H., and Wang, Q., 2021, "Redox Targeting of Energy Materials," Curr. Opin. Electrochem., **29**, p. 100743.
[39] Zhou, M., Huang, Q., Truong, T. N. P., Ghilane, J., Zhu, Y. G., Jia, C., Yan, R., Fan, L., Randriamahazaka, H., and Wang, Q., 2017, "Nernstian-Potential-Driven Redox-Targeting Reactions of Battery," Chem, **3**(6), pp. 1036–1049.
[40] Yu, J., Fan, L., Yan, R., Zhou, M., and Wang, Q., 2018, "A Redox Targeting-Based Aqueous Redox Flow Lithium Battery," ACS Energy Lett., **3**(10), pp. 2314–2320.
[41] Zhu, Y. G., Du, Y., Jia, C., Zhou, M., Fan, L., Wang, X., and Wang, Q., 2017, "Unleashing the Power and Energy of $LiFePO_4$-Based Redox Flow Lithium Battery With a Bifunctional Redox Mediator," J. Am. Chem. Soc., **139**(18), pp. 6286–6289.
[42] Pan, F., Huang, Q., Huang, H., and Wang, Q., 2016, "High-Energy Density Redox Flow Lithium Battery With Unprecedented Voltage Efficiency," Chem. Mater., **28**(7), pp. 2052–2057.
[43] Li, J., Yang, L., Yang, S., and Lee, J. Y., 2015, "The Application of Redox Targeting Principles to the Design of Rechargeable Li–S Flow Batteries," Adv. Energy Mater., **5**(24), p. 1501808.
[44] Zhu, Y. G., Jia, C., Yang, J., Pan, F., Huang, Q., and Wang, Q., 2015, "Dual Redox Catalysts for Oxygen Reduction and Evolution Reactions: Towards a Redox Flow Li–O_2 Battery," Chem. Commun., **51**(46), pp. 9451–9454.
[45] Zhu, Y. G., Wang, X., Jia, C., Yang, J., and Wang, Q., 2016, "Redox-Mediated ORR and OER Reactions: Redox Flow Lithium Oxygen Batteries Enable With a Pair of Soluble Redox Catalysts," ACS Catal., **6**(9), pp. 6191–6197.
[46] Zanzola, E., Dennison, C. R., Battistel, A., Peljo, P., Vrubel, H., Amstutz, V., and Girault, H. H., 2017, "Redox Solid Energy Boosters for Flow Batteries: Polyaniline as a Case Study," Electrochim. Acta, **235**, pp. 664–671.
[47] Zanzola, E., Gentil, S., Gschwend, G., Reynard, D., Smirnov, E., Dennison, C. R., Girault, H. H., and Peljo, P., 2019, "Solid Electrochemical Energy Storage for Aqueous Redox Flow Batteries: The Case of Copper Hexacyanoferrate," Electrochim. Acta, **321**, p. 134704.
[48] Zhou, M., Chen, Y., Salla, M., Zhang, H., Wang, X., Mothe, S. R., and Wang, Q., 2020, "Single-Molecule Redox-Targeting Reactions for a pH-Neutral Aqueous Organic Redox Flow Battery," Angew. Chem. Int. Ed., **59**(34), pp. 14286–14291.
[49] Cheng, Y., Wang, X., Huang, S., Samarakoon, W., Xi, S., Ji, Y., Zhang, H., et al., 2019, "Redox Targeting-Based Vanadium Redox-Flow Battery," ACS Energy Lett., **4**(12), pp. 3028–3035.
[50] Wong, C. M., and Sevov, C. S., 2021, "All-Organic Storage Solids and Redox Shuttles for Redox-Targeting Flow Batteries," ACS Energy Lett., **6**, pp. 1271–1279.
[51] Huang, H., Howland, R., Agar, E., Nourani, M., Golden, J. A., and Cappillino, P. J., 2017, "Bioinspired, High-Stability, Nonaqueous Redox Flow Battery Electrolytes," J. Mater. Chem. A, **5**(23), pp. 11586–11591.
[52] Pahari, S. K., Gokoglan, T. C., Visayas, B. R. B., Woehl, J., Golen, J. A., Howland, R., Mayes, M. L., Agar, E., and Cappillino, P. J., 2021, "Designing High Energy Density Flow Batteries by Tuning Active-Material Thermodynamics," RSC Adv., **11**(10), pp. 5432–5443.
[53] Bayer, E., Koch, E., and Anderegg, G., 1987, "Amavadin, an Example for Selective Binding of Vanadium in Nature: Studies of Its Complexation Chemistry and a New Structural Proposal," Angew. Chem. Int. Ed., **26**(6), pp. 545–546.
[54] Wang, B., Han, Y., Wang, X., Bahlawane, N., Pan, H., Yan, M., and Jiang, Y., 2018, "Prussian Blue Analogs for Rechargeable Batteries," iScience, **3**, pp. 110–133.
[55] Zhao, F., Wang, Y., Xu, X., Liu, Y., Song, R., Lu, G., and Li, Y., 2014, "Cobalt Hexacyanoferrate Nanoparticles as a High-Rate and Ultra-Stable Supercapacitor Electrode Material," ACS Appl. Mater. Interfaces, **6**(14), pp. 11007–11012.
[56] Potash, R. A., McKone, J. R., Conte, S., and Abruña, H. D., 2015, "On the Benefits of a Symmetric Redox Flow Battery," J. Electrochem. Soc., **163**(3), pp. A338–A344.
[57] Sinha, S., Humphrey, B. D., and Bocarsly, A. B., 1983, "Reaction of Nickel Electrode Surfaces With Anionic Metal-Cyanide Complexes: Formation of Precipitated Surfaces," Inorg. Chem., **23**(2), pp. 203–212.
[58] Sato, O., Einaga, Y., Iyoda, T., Fujishima, A., and Hashimoto, K., 1997, "Cation-Driven Electron Transfer Involving a Spin Transition at Room Temperature in a Cobalt Iron Cyanide Thin Film," J. Phys. Chem. B, **101**(20), pp. 3903–3905.
[59] Lezna, R. O., Romagnoli, R., de Tocconi, N. R., and Rajeshwar, K., 2002, "Cobalt Hexacyanoferrate: Compound Stoichiometry, Infrared Spectroelectrochemistry, and Photoinduced Electron Transfer," J. Phys. Chem. B, **106**(14), pp. 3612–3621.